Transactions of the Materials Research Society of Japan 31[2] 453-458 (2006)

Microplasma Integration and its Application to Atmospheric Pressure Thin Film Deposition

Osamu Sakai, Kunihide Tachibana, Kiyoshi Tatsugawa*, Katsuhiko Ohishi* and Ryouji Inoue*
Department of Electronic Science and Engineering, Kyoto University
Kyoto-daigaku Katsura, Nishikyo-ku, Kyoto 615-8510, Japan
Fax: 81-75-383-2290, e-mail: osakai@kuee.kyoto-u.ac.jp
*Hitachi Metals, Ltd., 2107-2, Yasugi-cho, Yasugi, Shimane 692-8601, Japan
Fax: 81-854-22-6374

Microplasmas integrated on one plane form a uniform two-dimensional plasma source working at atmospheric pressure of nitrogen and oxygen gases. Tetraethoxysilane flowing from an inlet on the side of the integration plane becomes dissociated and a uniform SiO_2 film is deposited on the counter side of the plane. Gas phase reaction process is discussed with gas flow geometry and nano-structured deposited layers.
Key words: microplasma, atmospheric pressure, deposition, remote plasma source, gas flow

1. INTRODUCTION

A microplasma, which has a size from mm to sub-micron, is inherently different from a conventional plasma generated at low pressure. Since it is by 1-3 orders smaller than the conventional one, its working gas pressure p in the vicinity of the minimum condition of ignition voltage lies around or more than atmospheric pressure according to the Paschen's law. Furthermore, it has high electron density more than 10^{12} cm^{-3} due to short electron mean free path and high dissipated electric power density. One of its technological advantages is easy integration on two-dimensional plane and in three-dimensional space. Integrated plasmas can create novel functions such as crystal-like behavior [1, 2] as well as enlarged reactive region.

In this report we focus on the uniform integration of microplasmas using N_2 and O_2 gases at atmospheric pressure and its application to thin film deposition of SiO_2 which is much influenced by gas flow geometry [3]. First application of SiO_2 film deposition at atmospheric pressure was by an ozone generator [4]. In this method, deposition rate as high as low-pressure plasma enhanced chemical vapor deposition was achieved, although reactor temperature had to be more than 400 °C. So as to realize more moderate condition, several atmospheric pressure plasma sources have been investigated [5, 6]. There have been several difficulties in achieving atmospheric pressure plasma processing, such as stability limitation coming from glow-to-arc transition and inhomogeneous distribution for large substrate processing. One of the adequate methods was realized in He dielectric barrier discharges [5], although He gas is so expensive for the usage of the atmospheric pressure processing. In our case, these two main problems, that is, stability and uniformity of a plasma source, can be removed by using integrated microplasmas, without He gas. Other large problem is excessive convective flow in contrast with diffusion transport, which is also optimized in this study.

In Section 2, experimental setup is described, and experimental results on discharge features, deposition rate and film properties are shown in Section 3. In Section 4, gas flow geometry is calculated and a gas-phase reaction model is proposed in our deposition reactor.

2. EXPERIMENTAL SETUP

A sheet-like plasma source with 44 mm x 44 mm area and perpendicular gas-flow structure, which was composed of integrated microplasmas, was designed for atmospheric pressure plasma processes [7]. A coaxial microhollow electrode structure was covered with a dielectric layer, and the opening of the unit hole was 200 μm x 1700 μm. A dielectric barrier discharge was ignited in this small hole between the stacked electrodes, and such microplasmas were assembled on one plane. Inlet gases flew through the holes where discharges took place, and became activated. The equivalent discharge path d between the two electrodes was several hundred μm in length, and relatively low discharge voltage is possible in such a low pd condition even at the

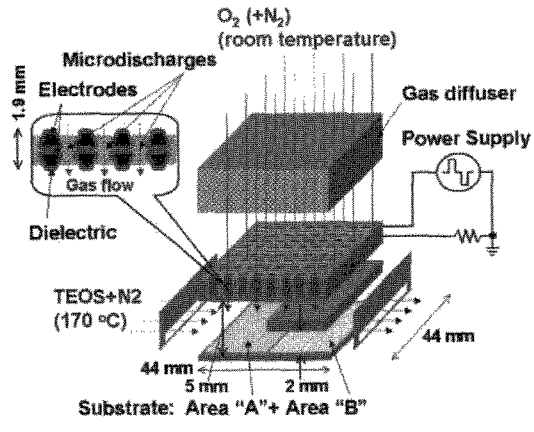

Fig. 1. Schematic view of reactor for SiO_2 deposition using integrated microplasmas. About 500 microplasmas are arranged on one plane. Deposition area "A" faces substrate surface, whereas gas flow channel becomes thin in front of deposition area "B".

atmospheric pressure.

Using this plasma source, we developed a remote-plasma-enhanced chemical vapor deposition reactor [3], as shown in Fig. 1. Tetraethoxysilane (TEOS) was vaporized at 170 °C in a liquid delivery system (PD-0-1, Japan Pionics), and its laminar flow carried by N_2 was combined with the gas flow dissociated by the plasma source. The predominant dissociation of TEOS is by electrons, O atoms, and O_3 molecules [8, 9] which are supplied from the integrated-microplasma plane. Gas flow rate was not so high (less than 10 litter per minutes (SLM)), leading to condition of the atmospheric pressure along all gas-flow paths including the plasma source region and the deposition area. In the deposition area, an inserted metal plate distinguished area "B" from area "A". In the cases of SiO_2 film deposition described later, the typical gas flowing through the microplasmas was O_2, and the gas of the laminar flow carrying TEOS was N_2. The applied voltage on the powered electrode was 2.1 kV_{0p} with 1-20 kHz bipolar square pulses, and discharge current was 2.2 A as a peak value.

Used substrates for deposition rate estimation by thin-film step-height standard method (XP-2, Ambious Technology) were plates of Fe and Ni alloy, and Si wafers were used for film bonding analysis by Fourier transform infrared (FT-IR) spectroscopy (WINSPEC100, JEOL). Surface morphology was observed by a normal scanning electron microscope (SEM, JSM-6060, JEOL). The substrate temperature was set to be 150 °C.

3. EXPERIMENTAL RESULTS

3.1 Discharge characteristics

Homogeneous distribution of visible emission was observed in pure N_2, pure O_2, and their mixture [3, 7]. Additional O_2 to N_2 raises ignition voltage, but its increase in pure O_2 was at most as high as 20 % of the pure N_2 case. Millimeter wave transmission method enables us to evaluate electron density n_e in this electrode configuration [10]. n_e in the pure N_2 or in the N_2 admixing with O_2 was 1-3x10^{12} cm^{-3}, and it decreased as O_2 ratio was raised. However, its decrease tendency was not so drastic, which implies that ne is around or slightly less than ~10^{12} cm^{-3} in pure O_2.

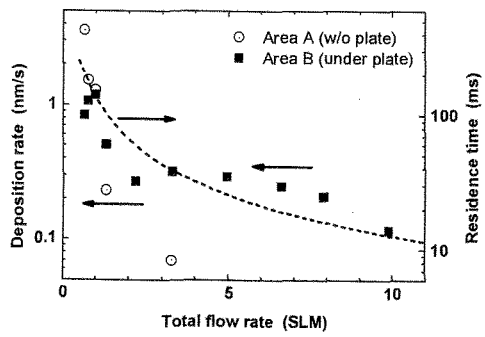

Fig. 2. Deposition rate at deposition areas A and B as a function of total gas flow rate. Residence time in area B is shown as an inset line.

3.2 Deposited film properties

When we investigated the gas flow rate dependence, we kept partial gas composition of each gas (O_2, N_2, and TEOS). We also varied frequency of the applied voltage pulses in proportional to the gas flow rate, which yielded to a condition where the input electric power in a unit of gas was kept constant. For instance, when the total gas flow rate was 6.6 SLM, O_2 flow rate was 3.6 SLM, N_2 carrying evaporated TEOS at 0.25 mg/min flew at the rate of 3.0 SLM, and the frequency of the power supply was set to be 14 kHz.

Deposition of SiO_2 thin film took place both in areas A and B, but a profile of the deposited film strongly depended on the gas flow rate, which is displayed in Fig. 2. When the total gas flow rate was more than 1 SLM, main deposition was in the area B, where channel thickness for the gas flow was limited to 2 mm. In general, convection flux, which is proportional to inlet

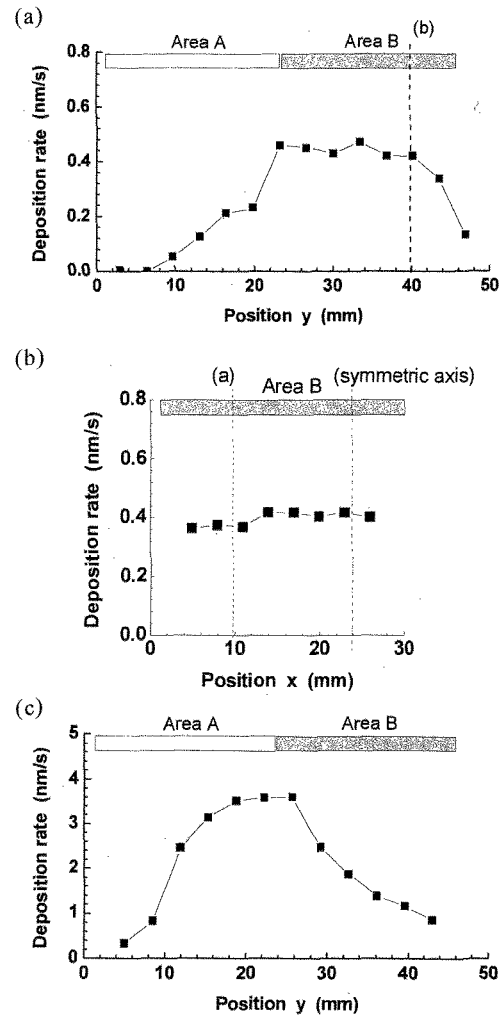

Fig. 3. Profiles of deposition rate on substrate. (a) Along gas flow at total gas flow rate of 1.3 SLM. (b) Across the gas flow at the total gas flow rate of 1.3 SLM. In these figures, the corresponding positions that the other figure displays are shown as inset lines. (c) Along the gas flow at the total gas flow rate of 0.66 SLM.

and outlet gas flow rate, is inversely proportional to residence time which enhances particulate formation through gas-phase reactions, so that the gas flow rate should be raised to avoid powder contamination in thin films at elevated pressure. On the other hand, diffusion flux toward the substrate which decreases as the pressure is raised due to reduction of diffusion coefficient. Consequently, diffusion flux in contrast to convection flux becomes smaller at elevated pressure, which leads to lowering deposition rate. In this sense, lower rate of the gas flow is required to keep deposition rate. One of the solutions to overcome this discrepancy is to enhance diffusion flux by making the flow thinner in the deposition area, which was realized in the area B.

In contrast, when the total flow rate was less than 1 SLM, main deposition was in the area A. As the flow rate became less than 1 SLM, the deposition rate in the area B decreased in the range. Deposition in the area A was never observed in the range of the total gas flow rate more than 4 SLM, whereas the deposition rate in the area A rapidly increased as the gas flow became slower for less than 2 SLM. If the above mentioned assumption about the ratio between the diffusion and the convection fluxes was valid, the deposition rate in the area B should increase even for 1 SLM, but that was not the case. Further analysis using the detailed gas flow geometry will be performed in Section 4.

Figure 3 displays the deposition profiles more clearly. Figures 3 (a) and (b) shows a profile of the deposited film in the case of the high flow rate in which main deposition took place in the area B. Near the gas inlet, no deposition occurred, and gradually the film thickness became large. In the area B, film thickness was two-dimensionally homogeneous. Figure 3 (c) shows a typical profile of the deposited film in the case of the low flow rate in which main deposition takes place in the area A. The film thickness increases rapidly from the

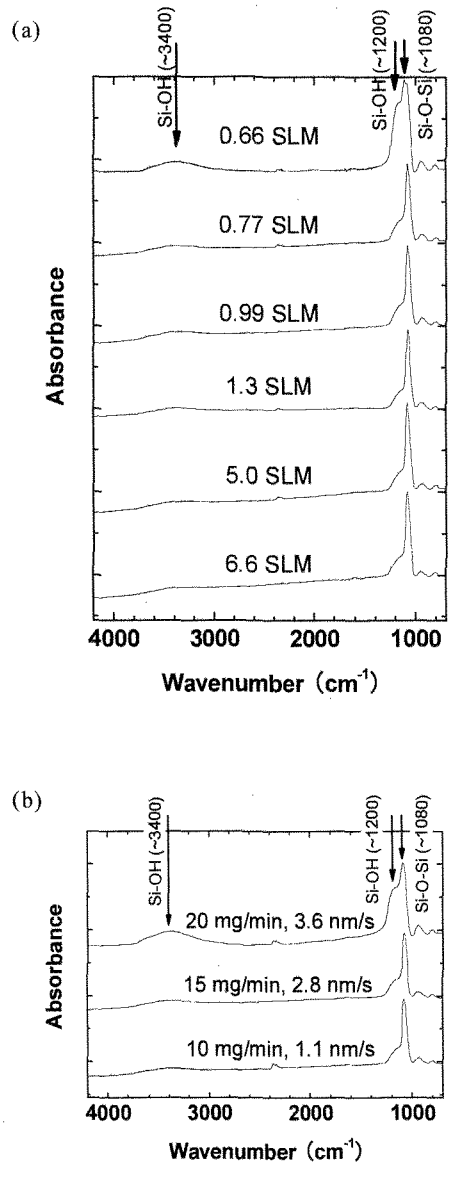

Fig. 4. FT-IR spectra (a) at area B as a function of total gas flow rate and (b) at area A as a function of TEOS flow rate with the total gas flow rate of 0.66 SLM.

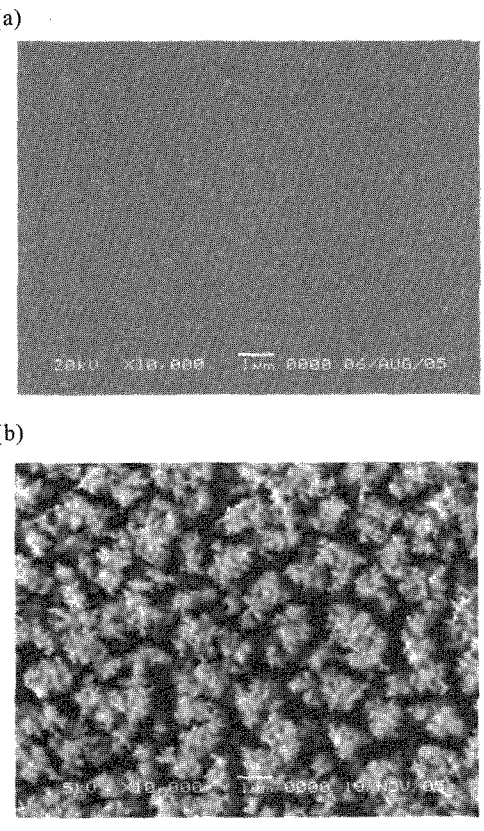

Fig. 5. (a) SEM images at deposition area "B" at total gas flow rate of 1.3 SLM with film thickness of 1 μm, and (b) at deposition area "A" at the total gas flow rate of 0.66 SLM with film thickness of 1.5 μm. An inset white bar indicates a unit scale (1 μm) in images.

inlet and got saturated in the area A. In the area B, the film thickness drastically decreased. This profile implies direct effect of the integrated-microplasma plane facing the area A.

FT-IR spectroscopy reveals film bond property of SiO_2 which has been extensively examined so far in a number of experiments. Figure 4 (a) shows gas flow dependence of FT-IR spectra corresponding to Fig. 1. Almost all spectra showed usual SiO_2 property without C-H bonds. One exception was in the case with the total flow rate of 0.66 SLM, where excessive Si-OH bonding signals at ~3400 cm^{-1} and ~1200 cm^{-1} were detected. Si-OH bonding is present on boundary surface of bulk SiO_2 structure, and so large amount of Si-OH bonding verifies a porous film. So as to depress the porous property in the case of the low flow rate, we changed only the TEOS flow rate with the constant O_2 and N_2 flow rates. Figure 4 (b) shows FT-IR spectra of the area A in the case of the low flow rate. As the TEOS flow rate was decreased, the signals resulting from Si-OH vanished and the spectra turned into typical ones for SiO_2 film bonding. That is, it is possible to obtain the condition of main deposition in the area A with good film property.

These presumptions were verified by SEM images, which are shown in Figs. 5 (a) and (b). In the case of the high flow rate, film surface in the area B was quite flat with very small roughness. On the other hand, film morphology at the area A showed tree-like nanostructure. Such fractal structure may result from production of large clusters in the gas phase by many inelastic collisions between intermediates.

4. DISCUSSION

4.1 Numerical derivation of gas flow geometry

Numerical analysis of gas flow distribution was performed by a solver for computational fluid dynamics (PHOENICS version 3.5.1, Concentration Heat & Momentum Limited) [11]. In brief, the general conservation equations of mass, momentum and energy are numerically solved using the finite volume method. It is capable of analyzing three dimensional gas flows, although we calculated two dimensional distribution in a cross section from the gas inlets to the outlet shown in Fig. 1, on the symmetric plane. From the inlet on the left wall, N_2 gas at 170 °C flows into the analysis space, and O_2 at 27 °C flows down from the inlet on the upper wall. Rigorously, N_2 flux carries TEOS particles, and O_2 flux includes O and O_3 fractions, but they are simplified into pure N_2 and pure O_2 flows, respectively. They are combined in the region corresponding to the area A, which we can denote "mixing region" here, and the mixture flows through the deposition area B under the inserted plate and goes out from the outlet on the right wall. To distinguish a fraction of O_2 from that of N_2, each continuum equation is written as, using the total mass density as ρ and the average velocity as $\boldsymbol{u}$,

$$\frac{\partial(C_\alpha \rho)}{\partial t} + \nabla \cdot (C_\alpha \rho \boldsymbol{u}_\alpha - D_\alpha \rho \nabla C_\alpha) = 0, \quad (1)$$

where C_α represents a fraction of a species in the mixture at each position, and $\alpha = N_2$ or O_2 with $C_{N2} + C_{O2} = 1$. Each D_α represents diffusion coefficient of a

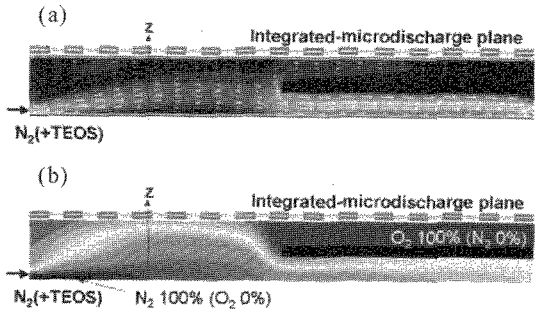

Fig. 6. Typical calculated profiles of (a) gas flow velocity and (b) O_2 concentration in the cross section along the gas flow. This is the case where total gas flow rate is 3.3 SLM. In (a), high velocity region (1.6 m/s at maximum) is expressed in white and white arrows indicate direction of velocity vectors. In (b), black regions indicate pure gas composition, whereas white regions show mixing region with 50% of N_2 and 50% of O_2.

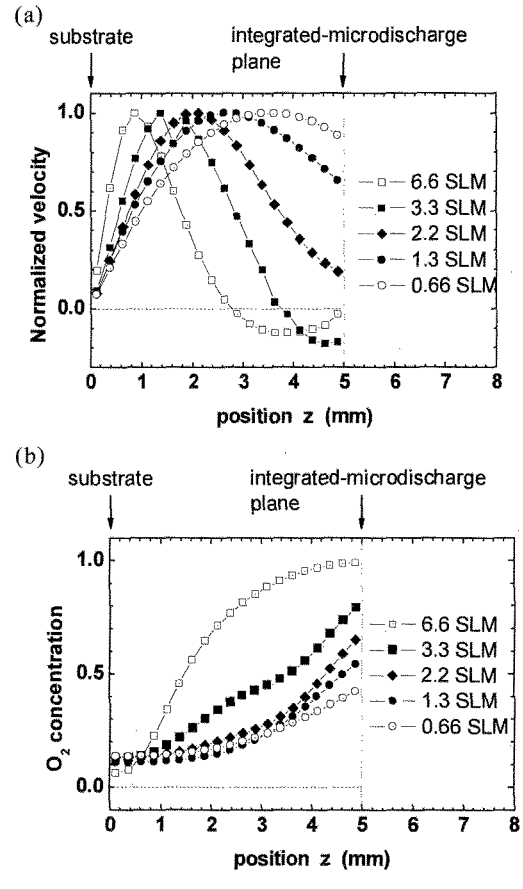

Fig. 7. (a) Profiles of gas flow velocity and (b) O_2 gas concentration as a function of gas flow rate along "z" line shown in Fig. 6 as inset lines.

species at 27 °C. In the specific calculation, Eq. (1) for O_2 species is solved and N_2 concentration is determined from the rest part of ρ. The lower wall can be considered as a substrate. Gas flow is assumed to be laminar one, and boundary condition on the walls is no-slip wall boundary. The unit calculation cell is 1.0 mm x 0.25 mm, and the fluid dynamics parameters in each cell depend on local composition of the gas species.

Figure 6 (a) shows a typical result on distribution of gas flow velocity in the case of the high gas flow rate (3.3 SLM). N_2 flux from the inlet flew over the area A into the area B where the flow channel was thin. From the integrated-microplasma plane, O_2 flux flew down and coalesced into N_2 in front of the area A. Figure 6 (b) indicates gas composition, where dark color corresponds to pure gas condition and white area indicates mixing region.

Figure 7 (a) displays velocity profiles in the area A across the gas flow as a function of the total gas flow rate. When the total gas flow was very high, velocity directions were reversed along the measured line, which means that N_2 flux with TEOS straightly proceeds to the area B. On the other hand, when the total gas flow was low, no reversed flow was present, and so N_2 flux admixed with O_2 and got contact with the integrated-microplasma plane. Such explanation is verified in Fig. 7 (b), where the gradient of the each gas concentration became gradual as the gas flow rate became slow. The gas composition near the integrated-microplasma plane showed mixing state, which was different from the case of the high total flow rate where pure O_2 condition was present.

These numerical results indicate that, in the case of the low gas flow, TEOS particles carried by N_2 attach with electrons and O atoms which are produced and present only in the vicinity of the microplasmas. As the result, decomposition of TEOS is enhanced in comparison with the non-attachment case. Created intermediates can reach the substrate due to low convective flow along the surface. Low velocity also enhances inelastic collisions between intermediates due to long residence time. That is why the deposition rate and the film thickness profile changes nonlinearly, and why the surface morphology changes drastically.

The configuration with relative high-flow rate, in which the main deposition takes place in the area B, has a wide parameter range of practical uses. Since the deposition area does not directly face the integrated microplasmas, elongation of the substrate area to further downstream region is possible to enlarge deposition area within the range where deposited film thickness is uniform. The inserted metal plate can be replaced by another substrate to make the output doubled. Furthermore, curved substrates can be dealt with if the channel thickness of the gas flow in front of the substrate is fixed. In these cases, the area of the integrated microplasmas becomes one of the controllable parameters for changing the amount of activated gas (O_3 in our case) density.

4.2 Evaluation of gas-phase reaction

Quantitative analysis about reaction rate is possible using rate constant if it is available from literature. Here a dominant radical species is discussed between O and O_3, where they interact with TEOS as [8, 9]

$$Si(OC_2H_5)_n(OH)_{4-n} + O \rightarrow Si(OC_2H_5)_{n-1}(OH)_{4-n+1} + CH_3CHO\,, \quad (2)$$

$$Si(OC_2H_5)_n(OH)_{4-n} + O_3 \rightarrow Si(OC_2H_5)_{n-1}(OH)_{4-n+1} + CH_3CHO + O_2\,, \quad (3)$$

where n = 1-4. To evaluate lifetime of each species, we consider these loss reactions as [9, 12]

$$O_2 + O + M \rightarrow O_3 + M\,, \quad (4)$$

$$O_3 + M \rightarrow O_2 + O + M\,, \quad (5)$$

$$NO + O_3 \rightarrow NO_2 + O_2\,. \quad (6)$$

From the reactions of (4)-(6) and assumed NO density with less than 10^{13} cm^{-3}, the lifetime of O_3 is more than 10 s, which means that O_3 is a long-life radical species surviving for over the residence time inside the reactor (< 1 s). On the other hand, the lifetime of O produced in the microplasmas via electron impact dissociation is about 5 μs, which corresponds to diffusion length < 1 μm along the gas flow. O radical species produced from O_3 via the reaction of (5) is present throughout the O_2 gas flow path, but they turn into O_3 via reaction (4) immediately and cannot to be the predominant decomposer for TEOS. We note that, on the surface of the integrated-microplasma plane, electron impact dissociation like

$$Si(OC_2H_5)_n(OH)_{4-n} + e \rightarrow Si(OC_2H_5)_{n-1}(OH)_{4-n+1} + C_2H_4 + e \quad (7)$$

is also of prime importance in addition to reactions (2) and (3).

Reaction of polymerization gives rise to nanoparticles as shown in Fig. 5 (b). Provided that they are in spherical shape of SiO_2 crystal, they are composed of several thousands of Si-O_2 trios. For instance, reaction of an oligomer as

$$Si(OC_2H_5)_2(OH)_2 + Oligo(OH)_2 \rightarrow Oligo(OH)_2 + H_2O \quad (8)$$

can create such a nanoparticle at the rate constant of $5x10^{-14}$ cm^3/s with the intermediate $Si(OC_2H_5)_2(OH)_2$ of $1.5x10^{15}$ cm^{-3} during its residence time of 0.13 s in the area A, on the assumption that 10% of the intermediates get together to form nanoparticles with the diameter of 100 μm. These derived values are in reasonable agreement with the experimental condition and the previous report [9].

5. CONCLUSION

We demonstrated, using micropalsma integration, two-dimensionally homogeneous SiO_2 film deposition at atmospheric pressure without He. Deposition rate profile over the whole substrate as well as the deposition rate itself drastically changed due to the total flow rate. Numerical analysis of fluid dynamics concluded that change of the gas flow geometry affected such phenomena. In this reactor configuration integrated

microplasmas work as an ozone generator and a TEOS decomposer, simultaneously.

ACKNOWLEDGMENTS

This work was supported partially by a Grant-in-Aid for Scientific Research from the Japanese Ministry of Education, Culture, Sports, Science and Technology and by an entrustment from the New Energy and Industrial Technology Development Organization.

REFERENCES

[1] O. Sakai, T. Sakaguchi, Y. Ito and K. Tachibana, *Plasma Phys. Contr. Fusion*, **47**, B617-B627 (2005).
[2] O. Sakai, T. Sakaguchi and K. Tachibana, *Appl. Phys. Lett.*, **87**, 241505 (2005).
[3] O. Sakai and K. Tachibana, *Proc. 17th International Symposium on Plasma Science* (Toronto, Canada, 2005) p. 240-241.
[4] K. Maeda and S. M. Fisher, *Solid State Technol.*, **6**, 83-88 (1993).
[5] Y. Sawada, S. Ogawa and M. Kogoma, *J. Phys. D: Appl. Phys.*, **28**, 1661-1669 (1995).
[6] S. E. Babayan, J. Y. Jeong, A. Schutze, V. J. Tu, M. Moravej, G. S. Selwyn and R. F. Hicks, *Plasma Sources Sci. Technol.*, **10**, 573-578 (2001).
[7] O. Sakai and K. Tachibana, *J. Phys. D: Appl. Phys.*, **38**, 431-441 (2005).
[8] M. A. Lieberman and A. J. Lichtenberg, "Peinciples of Plasma Discharges and Materials Processing", John Wiley & Sons, New York (1994) p.518-520.
[9] S. Romet, M. F. Couturier and T. K. Whidden, *J. Electrochem. Soc.*, **148**, G82-G90 (2001).
[10] K. Tachibana, Y. Kishimoto, S. Kawai, T. Sakaguchi and O. Sakai, *Plasma Phys. Contr. Fusion*, **47**, A167-A177 (2005).
[11] S. V. Patankar and D. B. Spalding, *Int. J. Heat Mass Transfer*, 15 1787-1806 (1972).
[12] F. Tochikubo and H. Arai, *Jpn. J. Appl. Phys.*, **41**, 844-852 (2002).

(Received December 12, 2005; Accepted March 29, 2006)